Development 130, 2543-2554

doi:10.1242/dev.00455

DEVELOPMENT AND DISEASE

Zebrafish *foxi one* modulates cellular responses to Fgf signaling required for the integrity of ear and jaw patterning

Robert M. Nissen[1], Jizhou Yan[2], Adam Amsterdam[1], Nancy Hopkins[1] and Shawn M. Burgess[2,*]

[1]Center for Cancer Research and Department of Biology, Massachusetts Institute of Technology, Cambridge, MA 02139, USA
[2]Genome Technology Branch, National Human Genome Research Institute, National Institutes of Health, Bethesda, MD 20892, USA
*Author for correspondence (e-mail: burgess@nhgri.nih.gov)

Accepted 20 February 2003

SUMMARY

We identified four insertional alleles of *foxi one* (*foo*), an embryonic lethal mutation in zebrafish that displays defects in both otic placode and the jaw. In *foo/foo* embryos the otic placode is split into two smaller placodes and mutant embryos show a dorsoventral (DV) cartilage defect manifested as a reduced hyomandibular and reduced third and fourth branchial arches. We identified *foxi one* (*foo*), the zebrafish ortholog of Foxi1 (FREAC6, FKHL10, HFH-3, Fkh10) and a member of the forkhead domain transcriptional regulator family, as the gene mutated in *foo/foo* embryos. *foo* is expressed in otic placode precursor cells, and *foo/foo* embryos lack placodal *pax8* expression and have disorganized otic expression of *pax2.1* and *dlx3*. Third stream neural crest cell migration, detected by *dlx2* and *krox20* expression, is aberrant in that it invades the otic placode territory. *foo* is expressed in pharyngeal pouch endoderm and is required for pouch expression of *pax8* and proper patterning of other markers in the pouch such as *nkx2.3*. In *foo/foo* embryos, we observed a failure to maintain *fgf3* expression in the pouches, followed by apoptosis of neural crest cells in adjacent arches. We conclude that *foo* expression is essential for *pax8* expression probably downstream of Fgf signaling in a conserved pathway jointly required for integrity of patterning in the otic placode and pharyngeal pouches. We propose that correct placement of survival/proliferation cues is essential for shaping the pharyngeal cartilages and that evolutionary links between jaw and ear formation can be traced to Fgf-Foxi1-Pax8 pathways.

Key words: Foxi1, Otic placode, Pharyngeal pouch, *fgf8*, *fgf3*, *pax8*

INTRODUCTION

We are using the zebrafish to study the genetic basis of ear and jaw development. Development of the zebrafish ear begins as a thickening of the epidermal layer into a two-cell-thick placode at the nine-somite stage (Kimmel et al., 1995). The placode cavitates to form a lumen and hair cells begin to differentiate, projecting bristles into the liquid filled interior (Haddon and Lewis, 1996). Over the next few days, columns of tissue grow out from the walls of the otic vesicle, fusing in the center of the space to generate semicircular canals. Many genes have been shown either to be expressed in the developing zebrafish ear, or to be involved in the proper formation of the organ (Whitfield et al., 2002). *pax2a* and *dlx3b* are expressed in the developing placodes and roles in ear development for each of these genes have been demonstrated or inferred (Krauss et al., 1991; Lun and Brand, 1998; Solomon and Fritz, 2002). Fgf3 and Fgf8 have been implicated directly in the induction of the otic placode (Leger and Brand, 2002; Maroon et al., 2002; Phillips et al., 2001). Inhibition of either one of these signaling molecules causes marked reductions in the size of the placode, while inhibiting both causes an elimination of the ear primordia. *pax8* is the earliest known molecular marker for cells that will become the otic placode, but its actual role in induction is not known (Pfeffer et al., 1998).

As in all vertebrates, the zebrafish ear serves the dual functions of linear acceleration detection and hearing (Bever and Fekete, 2002). Although functionally similar to the human ear, many structures are not present including the cochlea and middle ear. Remarkably, the middle ear structures first arose during the water-to-land transition and their origins are believed to be structures derived from the gills (spiracular pouch) and the jaw (hyomandibular bone) of fish (Webster et al., 1992).

The pharyngeal cartilages are derived from three streams of ventrolaterally migrating cranial neural crest (NC) cells. The pharyngeal skeleton shows both an anterior-to-posterior (AP) segmented polarity, with each segment deriving from an embryonic pharyngeal arch, as well as a dorsal-to-ventral (DV) polarity within individual AP segments (Trainor and Krumlauf, 2001). The first mandibular arch gives rise to a ventral Meckel's cartilage, which articulates with a dorsal

palatoquadrate. The second hyoid arch is serially homologous to the first arch with a ventral ceratohyal that articulates via the interhyal with the hyosymplectic. The hyosymplectic is composed of a ventral symplectic rod region and a dorsal plate-like hyomandibular region. The arches and pouches form dynamically with the ectoderm forming an AP series of bilateral surface 'in-pockets' complementary to bilateral endodermal out-pockets that together form the pharyngeal pouches separating adjacent arches along the AP axis. The migratory NC cells fill the spaces between the forming pouches adopting a cylindrical morphology encasing central cores of paraxial mesoderm (Kimmel et al., 2001).

Pharyngeal pouches likely signal to adjacent NC cells (Le Douarin and Ziller, 1993; Veitch et al., 1999) and essential roles for *endothelin1* (*edn1*) in forming ventral cartilages has been shown in zebrafish and mice (Clouthier et al., 1998; Kurihara et al., 1994; Miller et al., 2000). Evidence for a dorsal cartilage-patterning signal is provided by the zebrafish *fgf8* mutant, *acerebellar* (*ace*), which has a reduced hyomandibular region. However, early neural tube defects and absence of *ace* expression in the pouches makes interpretation difficult (Roehl and Nusslein-Volhard, 2001). Studies on zebrafish *casanova* (*cas*) mutants and Fgf3 morpholino antisense oligonucleotide knockdowns suggest that loss of Fgf3 pouch expression results in early apoptotic elimination of posterior NC cells (Alexander et al., 1999; David et al., 2002). How an Fgf signal might function in DV patterning within an arch is still unclear.

In a large, insertional mutagenesis screen performed at MIT (Amsterdam et al., 1999; Golling et al., 2002), we isolated four insertional alleles of the zebrafish ortholog of the forkhead related transcription factor Foxi1 (FREAC6, FKHL10, HFH-3, Fkh10) (Avraham et al., 1995; Chen et al., 2002; Clevidence et al., 1993; Hulander et al., 1998; Larsson et al., 1995) that show specific defects in both ear and jaw development. The otic placodes are severely reduced in size, often split into two smaller placodes, and the semicircular canals fail to form properly, often resulting in a single large cavity instead of the normal three distinct chambers. The dorsal first arch derivative, the palatoquadrate, is mildly reduced in mutant animals, whereas the ventral Meckel's cartilage is indistinguishable from wild type. The dorsal second arch derivative, the hyomandibular region, is severely reduced in mutant animals while the ventral symplectic rod region and ceratohyal appear only mildly affected. Of the posterior arches, the third and fourth arches show substantial variable reductions while the fifth to seventh branchial arch cartilages appear relatively unaffected. Interestingly, targeted mutations of Foxi1 in mice show defects in ear development and homozygous mutant mice are born with both hearing and vestibular defects, as well as a lower survival rate after birth (Hulander et al., 1998), suggesting some conservation of the developmental pathway of the ears between zebrafish and mice.

MATERIALS AND METHODS

Animal husbandry and cloning

Zebrafish were mutagenized, maintained and screened as previously described (Amsterdam et al., 1999). The retroviral insertion junction fragment cloning and animal genotyping procedures were as previously described (Golling et al., 2002; Sun and Hopkins, 2001). The primers used for genotyping carrier fish and embryos were:

1359A-link1 5′-CCGAGGACGCGCTTAAATTGGC-3′ and 1359A-link2 5′-GTCCACACACACACTGCATTTAAACATG-3′ in combination with nLTR3 5′-CTGTTCCATCTGTTCCTGAC-3′ for hi1321 and hi1359A;

1359A-link1 and 1321-0RT 5′-CTGATCCGTCCCGGTTGTATA-TGAGG-3′ in combination with RMN3′LTR 5′-GAGGAGACCCT-CCCAAGGAACAG-3′ for hi3239;

1321-start 5′-CCATATGACCGTGTATTGCGACTCCAACTTC-3′ and 3239-gap2 5′-AGACTGGAAGTGTCCGCCAATTTAAGC-3′ in combination with RMN3′LTR for hi3747.

Full-length cDNA for zebrafish *foo* was isolated by 5′-RACE and 3′-RACE as previously described (Golling et al., 2002). The primers used for 5′RACE amplification were 5′-GATGGTGCAGGTTC-TGCTGGTACATGCTG-3′ followed by 5′-TCTGACCTGCTGA-GTGTGCTCGTCTCTGAGG-3′. The primers used for 3′RACE amplification were 5′-GAGAAAAAGAAGAGCCGACGGAAAC-3′ followed by 5′-GTCTGTGAAATCCGAGGACGCG-3′.

Zebrafish BAC library screening

High-density filters to the CHORI-211 BAC library were hybridized with a radioactive probe made from the *Eco*RI-digested plasmid containing a partial *foo* cDNA. The positive BAC clones were identified by PCR amplifications and used for fingerprinting and automated sequencing.

RT-PCR

For RT-PCR analysis of *foo* gene expression in wild-type and mutant animals, embryos were collected according to a previously described staging method (Kimmel et al., 1995) and RNA was prepared using Trizol reagent (ROCHE) with subsequent first-strand synthesis as previously described (Sun and Hopkins, 2001). The RT-PCR primers used for amplifying the sequence containing all *foo* proviral insertion sites were 1321-start and 1321-RT2 5′-CCTAAGATGACAAGAA-TGGGTGTTGG-3′. For RT-PCR amplification of the internal non-flanking sequence the primers used were 3239-gap1 5′-CGCTC-AGTCAGATTTATCAGTACGTGG-3′ and 3239-gap2. The primers used for amplifying the β-actin control sequence were 5′-CATCA-GCATGGCTTCTGCTCTGTATGG-3′ and 5′-GACTTGTCAGTG-TACAGAGACACCCTG-3′.

Plasmids

The plasmid pCR2.1-foxi1 3′RACE was isolated by performing 3′RACE with the previously described primers. It was digested with *Not*I and antisense probe for in situ hybridization synthesized using T3 RNA polymerase as previously described (Sun and Hopkins, 2001). Previously described plasmids for probes were *hand2* (Angelo et al., 2000), *dlx2* and *dlx3b* (Akimenko et al., 1994), *gsc* (Schulte-Merker et al., 1994), *krox20* (*egr2* – Zebrafish Information Network) (Oxtoby and Jowett, 1993), *nkx2.3* (Lee et al., 1996) and *pax2a* (Krauss et al., 1991). Plasmid for making *fgf3* probe was constructed by PCR amplification from 0-24 hpf cDNA using primers fgf3-f 5′-CTTGTTGTTACTGAGCTTCTTGGATCCGAG-3′ and fgf3-r 5′-CCTCCAGATTTCAGTGTCAAACAATGCC-3′, followed by subcloning into pCRII-BLUNT to yield pCR-fgf3. To make antisense probe, pCR-fgf3 was digested with *Not*I and transcribed using SP6 RNA polymerase. Plasmid for making *pax8* probe was constructed by PCR amplification from 0-24 hpf cDNA using primers pax8-f 5′-GCTTCCGGAGGTGATCCGGCAAAGG-3′ and pax8-r 5′-CTG-GAGTTGGTGAATCTCCAGGCCTCG-3′ followed by subcloning into pCRII-BLUNT to yield pCR-pax8. To make antisense probe, pCR-pax8 was digested with *Bam*HI and transcribed using T7 RNA polymerase.

Embryo injections

Embryos were injected at the one- to four-cell stages using pulled glass needles and a picospritzer II (Parker Instrumentation) with the Fgf3-MO (Phillips et al., 2001). Calibration of injection needles

indicated an average injection volume of 1 nl per 50 msecond pulse. Morpholino sequence was 5′-ACTCATGTTGACTACTCCTCCCA-CT-3′; four-base mismatch control was 5′-ACTCATCTTCACTACT-GCTCCCAGT-3′.

In situ hybridization and immunohistochemistry

Whole-mount in situ hybridization was performed as previously described (Thisse et al., 1994). Two-color reactions were performed as previously described (Hauptmann and Gerster, 1995; Sun and Hopkins, 2001).

Whole-mount immunohistochemistry was performed as previously described (Hanneman et al., 1988).

For TUNEL assays, fixed dehydrated embryos were rehydrated and acetone permeabilized for 10 minutes at –20°C, then rehydrated in PBST, washed in PBS + 0.25 mg/ml BSA and preincubated in TdT buffer for 2 hours at room temperature. TdT/fluorescein-dUTP reactions (Roche product 1-767-291) were incubated overnight at room temperature. Embryos were then washed twice for 45 minutes in PBST+1 mM EDTA at 65°C, 4 times for 45 minutes in PBST at room temperature, and processed with anti-fluorescein antibodies for alkaline phosphatase activity as previously described (Thisse et al., 1994).

Cartilage staining

Alcian Blue staining was performed as previously described (Golling et al., 2002).

RESULTS

The zebrafish *foxi one* mutation has ear defects

We first identified *foxi one* (*foo*) as a mutant with a defect in ear development. The earliest morphologically detectable phenotype was a reduction in the otic placode size at around the 15-somite stage, with the placode appearing not only smaller, but split into two or more tiny placodes. These tiny placodes can later either fuse or remain split (Fig. 1B,D). When the placode was split into two smaller regions, an otolith typically formed in each otocyst (Fig. 1D).

foo/foo embryos are mutated in the forkhead related transcription factor Foxi1

Through established segregation analysis (Amsterdam et al., 1999), the mutant phenotype was linked to a single proviral integration for each of four independent isolates of *foo* (not shown). The genomic DNA adjacent to the proviral integration events was cloned, sequenced, and used to determine linkage of the insertions to the mutant phenotype (Fig. 1E) (see Golling et al., 2002) All alleles were crossed and failed to complement. Linkage data placed the mutation responsible for the *foo/foo* mutant phenotype within 0.9 cM of a proviral insertion. The sequences adjacent to all four proviruses show identity to a single zebrafish EST (Accession Number BI891904). We isolated several bacterial artificial chromosomes (BACs) and sequence from this genomic region showed significant homology at the DNA and protein level to the mouse forkhead related transcription factor Foxi1 (Fkh10) which has presumed orthologs in several species, including human (Fkhl10, FREAC6), rat (HFH-3) and frogs (Foxi1c). Among all species, including zebrafish, a genomic structure of two exons with a single intron (in the same location) is conserved (Fig. 1F). In one allele, hi3747, the mutagenic provirus lies in sequences encoding a poly-histidine stretch near the 5′ end of the gene and should result in a truncation before the conserved DNA-binding domain (Fig. 1F). We performed RT-PCR on mutant and wild-type embryos for each allele with two sets of primers: one set spanning the entire gene and located outside all four

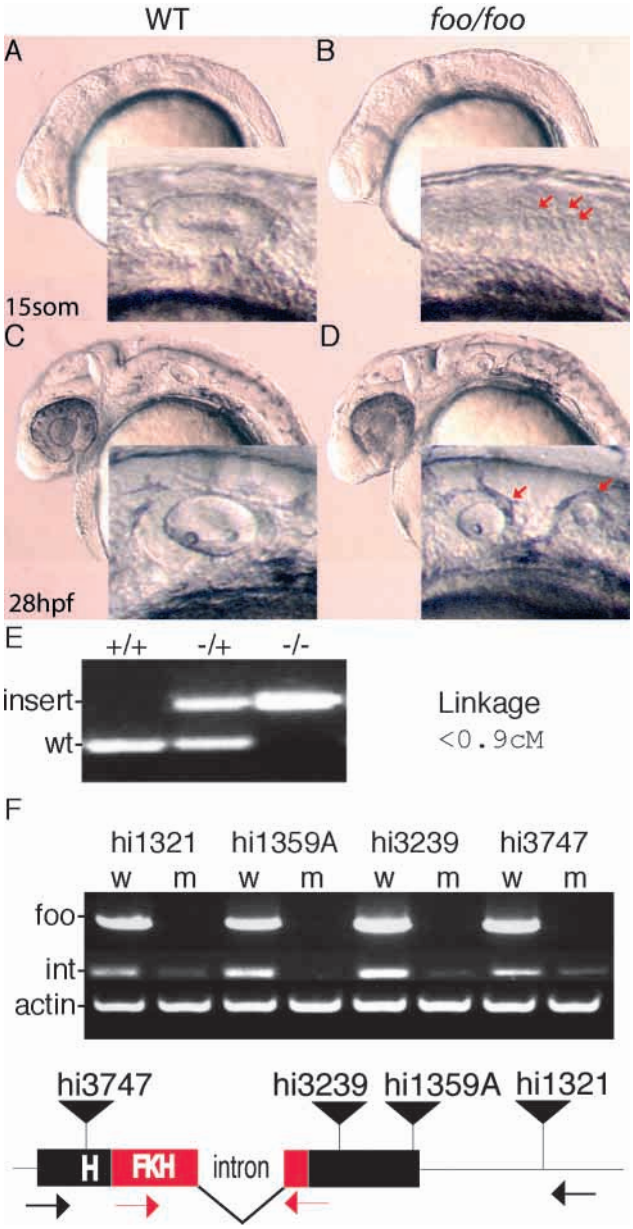

Fig. 1. Mutations in zebrafish *foxi one* cause defects in otic vesicle formation. (A) Lateral view of a wild-type embryo at 15 somites; inset is a magnification of the otic placode. (B) *foo/foo* embryo at 15 somites; arrows indicate putative placodes. (C) Wild-type ear at 28 hpf. (D) *foo/foo* embryo at 28 hpf; otic vesicle is clearly split into two smaller vesicles; arrows in inset indicate the two visible vesicles. (E) PCR products from genomic DNA indicating wild-type and mutant alleles of *foo* with the results of the linkage analysis in centimorgans. (F) RT-PCR analysis of each allele was performed. Wild-type, w; mutant, m. Bands marked *foo* use primers indicated by black arrows below; bands marked ‘int’ use primers indicated by red arrows. Integration for each allele is marked by a black triangle. The intron and the forkhead (FKH)-related DNA-binding domain are also indicated.

viral integration sites; and a second internal set that did not flank any of the viral integration sites (Fig. 1F). The longer amplicon was not successfully amplified from any of the alleles, although a significantly reduced amount of RNA was detected with the smaller amplicon in hi1321, hi3239 and hi3747. Almost no RNA was detected in the hi1359A allele. In situ hybridization of *foo* antisense RNA to mutant embryos was negative compared with wild-type siblings (Fig. 2D,E), suggesting a destabilized mRNA. The severity of the ear phenotype was variable within each mutant line, making comparisons of allele strength difficult. However, the allele with the most consistent phenotype was hi3747, the mutant with a proviral integration closest to the 5′ end of the gene and before the DNA binding domain. In hi3747, the otic vesicles were substantially reduced and often split (as in Fig. 1D).

Antisense oligonucleotides using morpholino chemistry have been shown to be effective, gene-specific, transcriptional inhibitors in zebrafish embryos (Ekker, 2000; Nasevicius and Ekker, 2000). As further confirmation that mutations in the *foo* gene are responsible for the observed phenotypes, we designed two morpholino antisense oligonucleotides to *foo* mRNA and injected them into embryos. In 50% of the embryos, the phenotype generated was indistinguishable from the mutant alleles (39/78) in ear or jaw defects, while the control morpholino showed no effect (data not shown).

Expression of Foxi1 in the early embryo

By RT-PCR, *foo* transcripts were not detected in unfertilized oocytes but were readily detected by the sphere stage (data not shown). Location of *foo* expression by in situ hybridization was first detected at the dome stage (Fig. 2A,B). By the shield stage, expression was in the presumptive ventral ectoderm near the animal pole that is fate mapped to be placodal precursors (Fig. 2C) (Kozlowski et al., 1997; Woo et al., 1995). By 90% epiboly, *foo* expression was split into bilateral regions (Fig. 2D). As convergence continued, *foo* expression appeared to be restricted to a region destined to become the otic placode (Fig. 2F). Expression of *foo* precedes expression of *pax8*, making it the earliest known marker of otic placode formation.

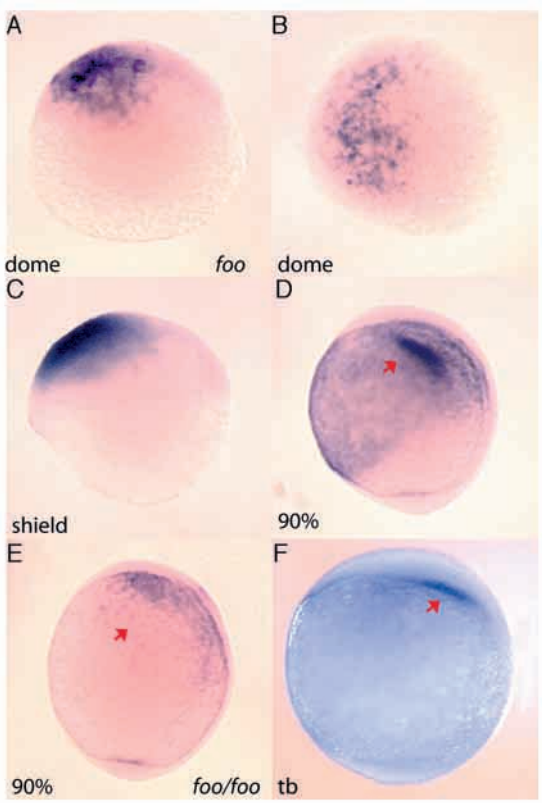

Fig. 2. Early expression of *foxi one* in the developing embryo. (A,B) Antisense RNA in situ hybridization of *foo* mRNA is first detected in the dome stage of embryos. (A) Lateral view; (B) dorsal view. (C) Lateral view of *foo* expression at the shield stage. (D) Lateral view 90% epiboly. Arrow indicates *foo* expression in the otic placode precursors. (E) Lateral view of a $foo^{hi3239}/foo^{hi3239}$ embryo, 90% epiboly. Arrow indicates loss of *foo* expression in the mutant embryo. (F) Lateral view tailbud stage; arrow indicates otic placode precursors expressing *foo*.

Impact of *foo* mutations on otic placode patterning

Because of the early expression of *foo* in the developing otic placode, we examined the expression in our mutant of other genes known to be expressed early in the otic placode. Mutant embryos showed reduced expression of *dlx3b* and *pax2a* that, in addition, was often split into several small patches of expression (Fig. 3D,F,H, arrows). Expression of *dlx3b* and *pax2a* in other areas of the developing embryo were unaffected (Fig. 3D,F,H, arrowheads). The strongest effect we detected was on the expression of *pax8*. At the one-somite stage, no *pax8* expression could be detected in the presumptive otic placode of one quarter of the embryos (Fig. 3B). However, we saw normal expression of *pax8* in the mesoderm of presumptive kidney (Fig. 3B, arrowhead). This suggests that *foo* is upstream of *pax8* in the otic vesicle and is required for proper expression of *pax8* in this region.

foo/foo embryos display defects in neural crest cell migration

dlx2 is normally expressed in all three streams of migratory NC cells beginning around the two- to three-somite stage. NC cells migrating out of rhombomere 5 (r5) normally move ventrally in a posteriolateral arc around the otic placode (Fig. 4A, arrow). Because the *foo/foo* mutant embryos displayed a significant disruption in otic placode development, we examined markers of migratory neural crest cells to determine whether disrupting the otic placode might affect normal NC cell migration. In *foo/foo* embryos the intensity of *dlx2* expression was normal but the third stream NC cells appeared slightly more anterior and no longer distinct from the second stream (Fig. 4B, arrowhead). *krox20* is expressed only in third stream migratory NC cells exiting r5. In *foo/foo* embryos, these NC cells migrated ventrolaterally, but failed to make the posterior movements around the otic placode (Fig. 4, compare C with D, arrowheads). Many cells were observed migrating through the otic placode region. Notably, the anterior margin of the post-migrating third stream NC cells has only shifted minorly towards the anterior (Fig. 4E,F arrows). In addition, the migration of second stream NC cells was indistinguishable from wild type, as visualized by *ephrin B2a* (*efnb2a*) expression (data not shown). It is unclear whether these changes are the result of a reduced otic placode or loss of *foo* expression. Cell transplantations will be required to answer this question.

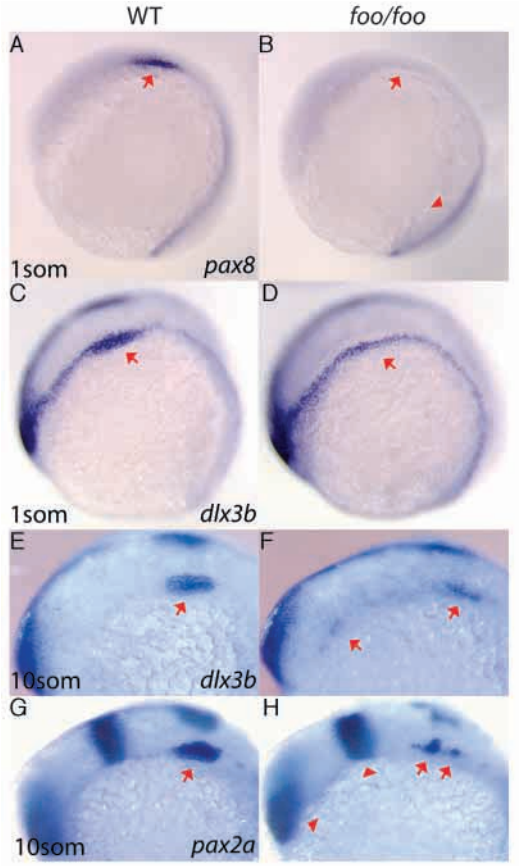

Fig. 3. Effects of the *foxi one* mutation on otic placode markers. Right panels, *foo/foo* homozygote embryos; left panels, same-clutch wild-type siblings. (A,B) Lateral view of *pax8* expression in wild-type (A) and *foo/foo* (B) one-somite stage embryos. Arrows indicate otic placode region. Arrowhead (B) indicates normal presumptive kidney staining. (C,D) Lateral view of *dlx3b* staining in one-somite stage wild-type (C) and a *foo/foo* (D) embryos. Note only otic placode expression is altered in the mutant. (E,F) *dlx3b* staining in 10-somite stage wild-type (E) and *foo/foo* (F) embryos. Arrow in E indicates otic placode. Arrows in F indicate scattered staining. (G,H) *pax2a* expression in 10-somite stage wild-type (G) and *foo/foo* (H). Arrows indicate scattered otic placode expression in mutant. Arrowheads indicate normal mid-hindbrain boundary and eye expression.

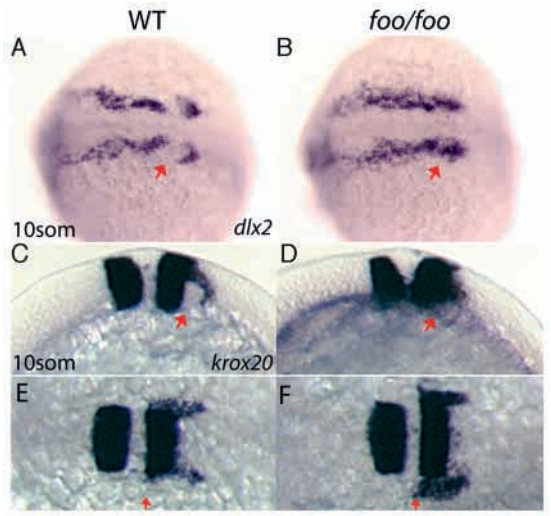

Fig. 4. *foxi one* mutants display defects in third stream neural crest migration. Right panels, *foo/foo* homozygote embryos; left panels, same-clutch wild-type siblings. (A,B) Dorsal view of *dlx2* expression in wild-type (A) and *foo/foo* (B) 10-somite stage embryos. Arrow in A indicates third stream NC cell migration avoiding the otic placode territory. Arrow in B indicates third stream NC cell invasion of the otic placode territory. (C,E) Lateral (C) and dorsal (E) views of *krox20* staining in a 10-somite stage wild-type embryo. Arrows indicate NC cells streaming in a posterior and lateral direction. (D,F) Lateral (D) and dorsal (F) views of a 10-somite stage *foo/foo* embryo. Arrow in D indicates NC cells invading otic placode territory. Arrow in F indicates approximately normal anterior border for *krox20*$^{+}$ NC cells.

Impact of *foxi one* mutations on jaw development

By 5dpf, *foo/foo* embryos display significant defects in the cartilaginous structures of the developing jaw (Fig. 5A,B), observable from both lateral and ventral views (Fig. 5C-F). Most notably in all hi3747 embryos, there is a severe reduction of the hyomandibular region (Fig. 5C,D, labeled hm). As it is often difficult to see this reduction, we flat-mounted the jaw cartilage to illustrate better the loss of the hyomandibular (Fig. 5G,H). We also saw variable reductions in the ceratohyals (ch) (strong example of reduction in Fig. 5F), and third and fourth gill arches (Fig. 5, numbers). Ceratohyal inversion is a common phenotype seen in back arch mutants. Therefore, inversion of the ceratohyals in *foo/foo* embryos probably results from the reduced third and fourth arches. There is a subtle, but consistent reduction in the overall measured size of the palatoquadrate (PQ) (Fig. 5I), although there is no apparent reduction in the more ventral Meckel's cartilage (M) (Fig. 5I). The embryos die after 6-7 days from unknown causes that are presumed to be related to the phenotypes either observed or yet to be determined. Injection of high concentration *foo* antisense morpholinos generated a morphant phenocopy of the jaw defects (data not shown).

Foxi1 expression during pharyngeal arch development

To begin to investigate the roles *foo* plays during jaw development, we examined expression of *foo* at later developmental time points. By the 10 somites stage, expression in the otic placode has faded and a second region of expression more ventral and lateral is apparent (Fig. 6A,B). Double staining of 10-somite stage embryos with *krox20* and *foo* shows that a stream of ventroanteriorly migrating *foo*-positive NC cells can be detected that are probably second stream associated NC cells. These *foo*-positive cells appear to initiate expression of *foo* as they approach their ventrolateral destinations, and suggest that *foo* is expressed in at least a subset of the post-migratory second stream NC (Fig. 6E, arrows). Initiation of *foo* expression was likewise detected among post-migratory third stream NC cells. However, second arch associated NC cell expression of *foo* is significantly downregulated by the 15-somite stage and no longer detected by 24 hpf (Fig. 6B,D). By the 15-somite stage, *foo* expression is readily detected in the region of what will be endodermal precursor cells of the first and second pharyngeal pouches (pp1, pp2 in Fig. 6B,C). *foo* expression remains strong in this region at least until 32 hpf, with downregulation proceeding in a medial-to-lateral and

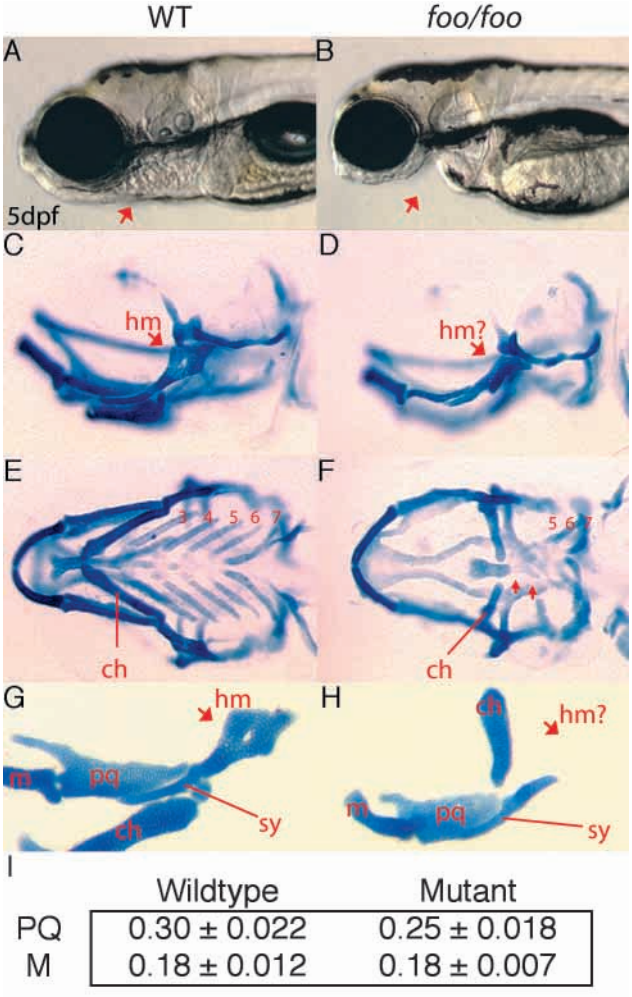

Fig. 5. *foo* mutants display defects in cartilages of the second, third and fourth pharyngeal arches. (A,B) Lateral views of wild-type (A) and *foo*/*foo* (B) embryos at 5 dpf. Arrow indicates jaw defects. (C,D) Lateral views of wild-type (C) and *foo/foo* (D) embryos at 5 dpf; wholemounts, Alcian Blue stained cranial cartilages. Arrow in D indicates the reduced hyomandibular region (hm) of the hyosymplectic. (E) Ventral view of C. The ceratohyal (ch) is indicated and gill arches are numbered 3-7. (F) Ventral view of D. The mildly reduced ch is indicated and arrows indicate the severely reduced third and fourth arch cartilages. The remaining gill arches 5-7 are indicated. (G) Flatmount of animal in C. Arrow indicates the hm region; line indicates the symplectic rod region (sy). The palatoquadrate (pq), Meckel's (m) and ch are also indicated. (H) Flatmount of animal in D. Arrow indicates the reduced hm while a line indicates the relatively normal sy. In *foo/foo* flatmounts, the ch positions abnormally because of an apparent defect in the articulation between ch and the hyosymplectic. (I) Chart comparing the measured length of the palatoquadrate (PQ) and Meckel's (M) cartilage in wild-type and *foo* mutant embryos. Measurements were made of eight wild-type and six mutant embryos. The palatoquadrate shows a small but measurable reduction in size in *foo* mutants.

anterior-to-posterior fashion. Transverse sections through pp1 verified endodermal expression (Fig. 6F).

Absent cartilages reflect lost NC-cell marker-gene expression domains

As the cartilages are derived from NC cells, we examined the expression patterns of early NC cell markers. *dlx2* is expressed in both migrating NC cells and post-migratory arch-associated NC cells. At 28 hpf, we detected a substantial reduction of *dlx2* expression in *foo/foo* embryos in the NC cells that populate the third and fourth arches, both of which are derived from third stream NC cells (Fig. 7A,B). Analysis of *dlx3b* expression, which is also expressed in post-migratory NC cells, revealed reduction of expression in the third and fourth arches in *foo/foo* embryos (data not shown). The endothelin 1 signaling pathway is essential for the proper formation of ventral cartilages and at least partly functions through the induction of the transcription factor *hand2* in ventral NC cells (Miller et al., 2000). The ventral expression of *hand2* appeared largely unaffected in the first and second arches consistent with the near normal formation of ventral cartilage elements in the anterior arches, but, mirroring the *dlx2/3* defects, expression of *hand2* was markedly reduced in the third and fourth arches of *foo/foo* embryos (Fig. 7C,D). Taken together, altered expression in *foo/foo* embryos of these three markers indicate a severe disruption in the proper patterning of the third and fourth arches.

The hyomandibular region of the hyosymplectic is reduced in *foo/foo* embryos. This element is derived from dorsal second arch NC cells. Because the *dlx2* and *dlx3b* data indicate a reduction in dorsal second arch NC cell expression, the dorsally and ventrally second arch restricted transcription factor *gsc* was examined for potential dorsal-specific defects (Schulte-Merker et al., 1994). *gsc* expression in wild-type embryos shows distinct dorsal NC cell expression in the first and second arches flanking either side of pp1 as well as a distinct second arch ventral expression domain (Miller et al., 2000). Outside the arches, *gsc* is also expressed within the developing otic vesicle. Strikingly, the dorsal first and second arch *gsc* expression domains were not detected in *foo/foo* embryos (Fig. 7E,F, arrows). Expression in the otic vesicles was likewise not detected in *foo/foo* embryos. Conversely, the olfactory and ventral second arch *gsc* expression domains appeared unaffected in mutants. Consistently, the homeobox transcription factor *hoxa2*, which is uniformly expressed in the second arch NC cells, also showed a dorsally restricted second arch NC cell defect (data not shown). Thus, defects in markers for the dorsal, but not ventral, NC cells of the first and second arches precedes the hyomandibular defect.

foo is required for survival of certain NC cell populations

To determine whether the loss of expression of NC cell markers and absence of corresponding cartilages was the result of NC cell apoptosis, we performed terminal deoxynucleotidyl transferase fluorescein-dUTP nick end labeling (TUNEL) assays to visualize apoptotic cells in developing embryos. When compared with wild-type embryos, *foo/foo* embryos display a substantial, transient increase in apoptosis in the pharyngeal arch region (Fig. 8A-G). The transient wave of cell death peaks around 26 hpf at ~20-fold over the intensity observed in wild-type embryos, and is then reduced by 28 hpf (Fig. 8H). Notably, no increased apoptosis was observed at 22 hpf or at earlier time points during otic development (Fig. 8H; data not shown). Based on their sub-ectodermal location in transverse sections, at least some of these TUNEL-positive cells appear to be post-migratory NC cells (Fig. 8E-G, sections located as approximately indicated in 8D). However, we cannot

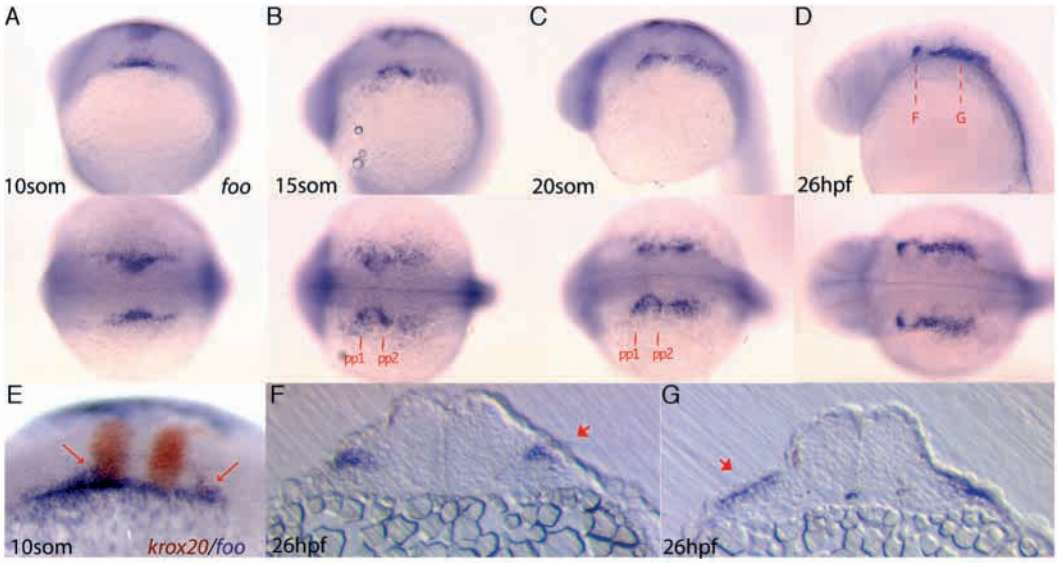

Fig. 6. Expression of *foo* at later stages of development. Detection of *foo* transcripts in later stages of wild-type embryos. Expression is consistent with both NC cell and future pharyngeal pouch endoderm expression. (A-D) lateral view (top) and dorsal view (bottom) of *foo* expression at different stages of development. (A) 10-somite stage. (B) 15-somite stage; pharyngeal pouch endoderm of pp1 and pp2 are indicated. (C) 20-somite stage. (D) 26 hpf; broken red lines indicate location of sections shown in F,G. (E) Double in situ hybridization to *krox20* and *foo* in a 10-somite stage embryo. Arrows indicate *foo* expression in streaming NC cells. (F) Transverse section of a 26 hpf *foo* in situ hybridized embryo through pp1. Arrow indicates endodermal pouch expression. (G) Transverse section of a 26 hpf *foo* in situ hybridized embryo through the post-otic region. Arrow indicates *foo* expression.

rule out that some of these TUNEL-positive cells might be endodermal pouch cells.

Foxi1 is required for normal pharyngeal pouch patterning

Fibroblast growth factors (Fgfs) are known to have mitogenic activity and *fgf3* is known to be expressed in the posterior half of pharyngeal pouches (David et al., 2002). Therefore, we examined the dynamic expression of *fgf3* in the pharyngeal pouches. By 15 somites to at least 34 hpf of development, *fgf3* was expressed in the endoderm two pouches at a time with downregulation in the most anterior pouch coincident with up regulation in the next most posterior pouch on a roughly four hour cycle (Fig. 8I,K,M,O, arrowheads; data not shown). At 16- and 20-somite stages, expression of *fgf3* was not significantly different between wild-type and mutant animals indicating that initiation of *fgf3* expression was not compromised, and that *fgf3*-positive cells are at least initially present in mutant animals (Fig. 8I,J). However, by the 24-somite stage, *foo/foo* embryos showed a premature loss of *fgf3* expression from pp1, the anterior-most pharyngeal pouch (Fig. 8L, red arrowhead). Examination of later developmental time points also shows premature loss of *fgf3* expression from the anterior-most pouch (Fig. 8N,P, blue then first black arrowhead). Thus, although initiation of *fgf3* pouch expression is always observed, the maintenance of *fgf3* pouch expression appears compromised. Expression of *fgf3* in other regions of the embryo, such as the isthmic region, was unaffected, which indicates the specificity of this defect.

As morpholinos that inhibit *fgf3* are known to cause posterior pharyngeal arch defects similar to those observed in *foo/foo* embryos, we analyzed *fgf3* morpholino injected animals for hyomandibular defects (David et al., 2002). Consistent with personal communications (L. Maves and C. B. Kimmel, unpublished) we observed not only the posterior gill

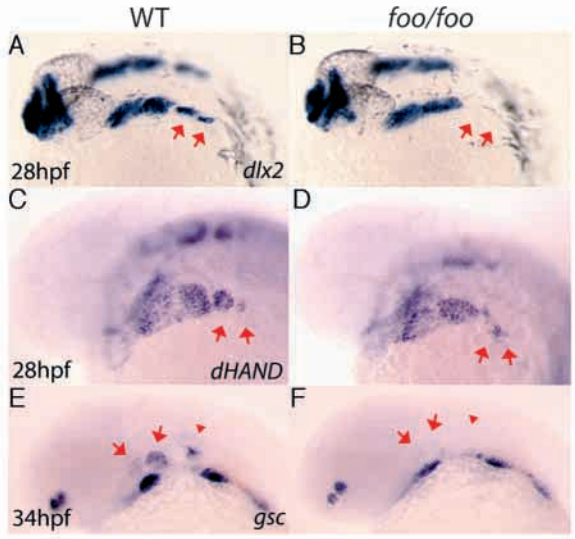

Fig. 7. *foo* mutants show post-migratory NC cell defects. Right panels, *foo/foo* homozygote embryos; left panels are same-clutch wild-type siblings. (A,B) *dlx2* expression by in situ hybridization in wild-type (A) and *foo/foo* (B) 28 hpf embryos. Arrows indicate third stream derived third and fourth arch NC cells. Note the apparent loss of the third and fourth arch expression domains in the mutant. (C) *hand2* expression by in situ hybridization in wild-type (C) and *foo/foo* (D) 28 hpf embryos. Arrows indicate third stream derived third and fourth arch NC cells. Note the reduction and disorganization of the third and fourth arch expression domains in the mutant. Also note the normal ventral expression of *hand2* in the first and second arches. (E,F) *gsc* expression by in situ hybridization in wild-type (E) and *foo/foo* (F) 34 hpf embryos. Arrows in E indicate dorsal *gsc* expression domains in the first and second arch NC cells flanking either side of pp1. Arrowhead in E indicates *gsc* expression in the otic vesicle. Arrows in F indicate where *gsc* expression can no longer be seen in the more dorsal region of expression; more ventral domains remain in *foo* embryos. Otic vesicle expression is also absent (arrowhead in F).

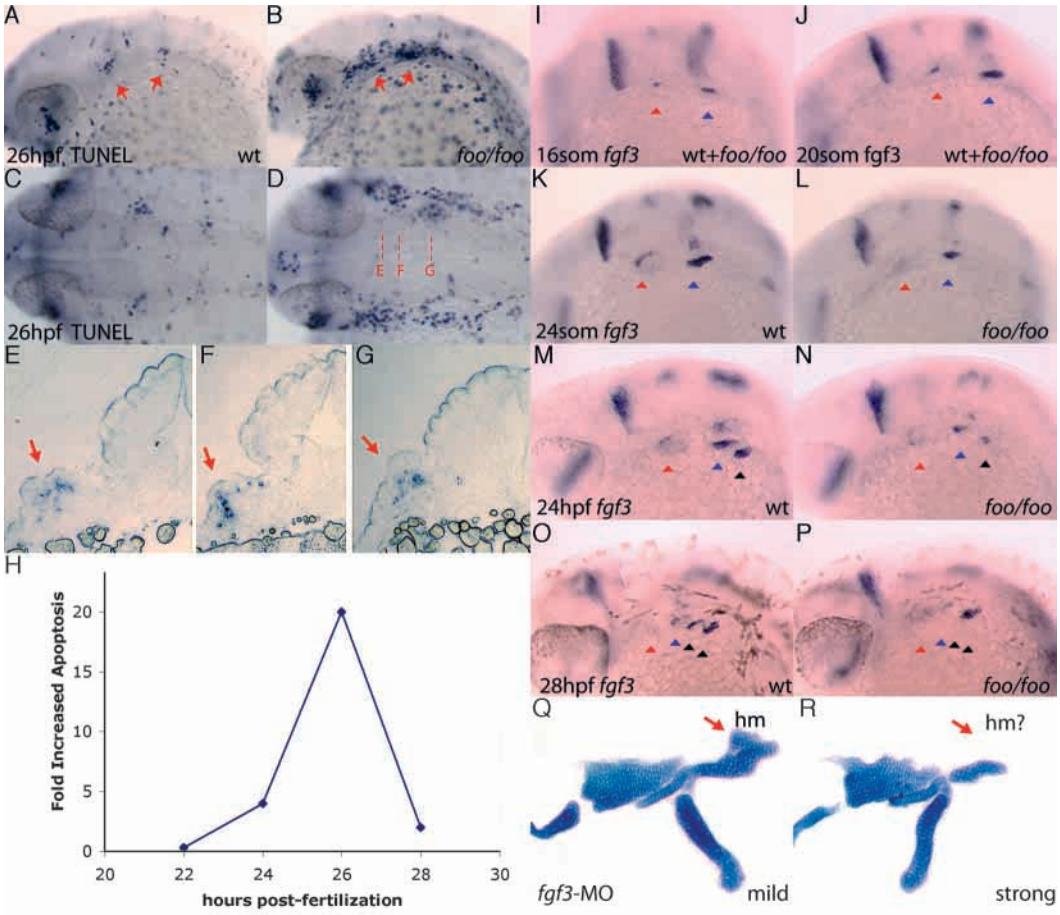

Fig. 8. *foo* mutants show a loss of *fgf3* expression maintenance in the pharyngeal pouches and increased apoptosis. (A,B) TUNEL assay on a wild-type (A) and *foo*/*foo* (B) embryos at 28 hpf, lateral views. Arrows indicate pp1 and pp2 with increased apoptosis. (C) Dorsal view of A; (D) dorsal view of B. Broken lines indicate approximate section locations. (E-G) Sections of TUNEL assay stained *foo*/*foo* embryos indicated in D. Arrows indicate TUNEL-positive cells. (H) Transient increase in apoptosis observed in *foo*/*foo* embryos. Quantitation was performed using NIH-Image for densitometry analysis of corresponding arch regions between mutant and wild-type embryos. Data points represent averages for at least three embryos. (I-P) *fgf3* expression by in situ hybridization in *foo*/*foo* (I,J,L,N,P) and wild-type (I,J,K,M,O) siblings. (I) 16-somite stage (mutants are indistinguishable from wild type at this stage). (J) 20-somite stage (mutants can not be distinguished from wild type). (K) 24-somite stage embryo. *fgf3* expression is maintained in pp1 (red arrowhead) and pp2 (blue arrowhead). (L) 24-somite stage. *fgf3* expression maintenance is lost from pp1, while pp2 expression is slightly lower than in wild type (K), but clearly visible. (M) 24 hpf embryo. *fgf3* expression is maintained in pp2 (blue arrowhead) and pp3 (black arrowhead). (N) 24 hpf embryo. *fgf3* expression maintenance is reduced from pp2 and initiation is visible in pp3. (O) 28 hpf embryo. *fgf3* expression is absent from pp1 (red arrowhead), is downregulated in pp2 (blue arrowhead), maintained in pp3 (left black arrowhead) and initiated in pp4 (right black arrowhead). (P) 28 hpf embryo. Expression is initiated normally in pp4 (second black arrowhead) but is prematurely lost from pp2 (blue arrowhead) and pp3 (left black arrowhead). (Q) Flat-mounted Alcian Blue staining of a mildly affected 4 dpf embryo injected with 5 ng of *fgf3*-MO (Phillips et al., 2001). Hyosymplectic (red arrow) appears relatively normal. (R) A more strongly affected 4 dpf embryo injected with 5 ng of *fgf3*-MO shows a reduction in the hyosymplectic (red arrow) consistent with the skeletal defects observed in *foo/foo* embryos.

arch defects but also a reduction of the hyosymplectic (Fig. 8Q,R, arrows). Out of 39 *fgf3* morpholino-injected animals selected at 30 hpf for a reduced otic vesicle phenotype and raised to 4 days of age, 10 showed all cartilages severely reduced (not shown), 16 displayed the strong phenotype (Fig. 8R) and 13 showed the mild phenotype (Fig. 8Q). We also analyzed *fgf3* morpholino injected animals for apoptosis by TUNEL assay and observed substantially increased levels of apoptosis in morphant animals compared with controls. However, extensive cell death in *fgf3* morpholino injected animals made conclusive interpretations of the TUNEL assays regarding specific NC cell apoptosis effects difficult (data not shown).

To determine the extent of the pharyngeal pouch patterning defect, we examined the staining pattern of zn-8, a monoclonal antibody that recognizes the pouch ectoderm, and we examined the expression pattern of the transcription factor *nkx2.3*, a later marker for posterior pouch endoderm. At 34 hpf, the zn-8 antibody effectively labeled pp1-pp4 in the wild-type animal but *foo/foo* embryos displayed significant reductions in pp2-pp4 (Fig. 9A,B). Although slightly reduced, pp1 was labeled by zn-8 in *foo/foo* embryos indicating that complete patterning of pp1 may depend upon additional factors, reflecting the higher complexity of the cartilage structures developing adjacent to this pouch. Consistent with this interpretation, *ephrin B2a* expression in pp1 was unaffected in *foo/foo* embryos (data not shown). The disrupted expression of *nkx2.3* from pp2-pp5 provides further indication that posterior pouch patterning requires *foo* (Fig. 9C,D).

Conserved *foo/pax8* signaling in the pharyngeal pouches

Expression of *pax8* has been reported in the hyoid arch in mice, but has not been reported in the zebrafish hyoid arch (Pfeffer et al., 1998). To determine whether the *foo-pax8* pathway is present in the pharyngeal pouches we examined *pax8* expression in *foo/foo* embryos. Although we were unable to detect expression of *pax8* in pp1 or pp2 at the 15-somite stage (data not shown),

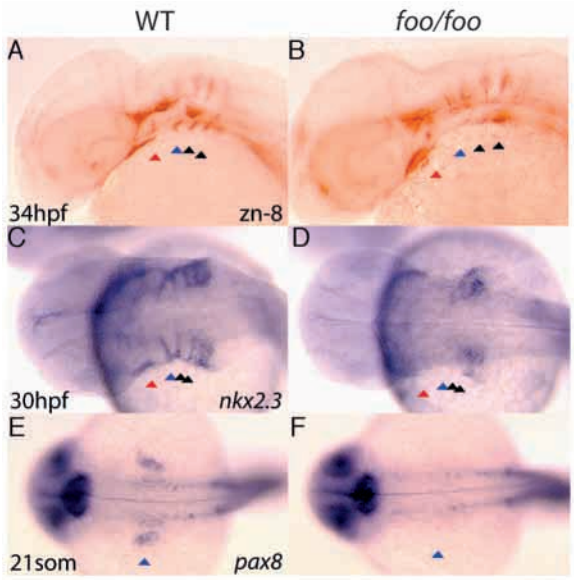

Fig. 9. The *foo* mutation affects pouch formation. Right panels, *foo/foo* homozygote embryos; left panels, same-clutch wild-type siblings. (A) zn-8 antibody staining of a wild-type embryo at 34 hpf. Pharyngeal pouches (pp1-pp4) are indicated by arrowheads as in Fig. 8. (B) zn-8 antibody staining of a 34 hpf *foo/foo* embryo. The posterior pouches pp2-4 are substantially reduced, whereas pp1 is only mildly affected. (C) *nkx2.3* expression by in situ hybridization of a 30 hpf wild-type embryo. (D) *nkx2.3* expression in a 30 hpf *foo/foo* embryo. Most of the *nkx2.3* expression is absent or disorganized. (E) *pax8* expression in a 21-somite wild-type embryo with pp2 indicated as in A. (F) *pax8* expression in a 21-somite *foo/foo* embryo. Expression of *pax8* in pp2 is absent and the otic vesicle is substantially reduced.

there was clear expression of *pax8* in the posterior part of pp2 at the 21-somite stage and that expression domain was absent in *foo/foo* embryos (Fig. 9E,F, blue arrowhead). Likewise, at 30 hpf, *pax8* expression was observed in more posterior pouches of normal sibling embryos but absent in *foo/foo* embryos (data not shown). This apparent AP progression of *pax8* pouch expression was reminiscent of both the *foo* and *fgf3* expression profiles. Interestingly, at 34 hpf, *pax8* expression in the thyroid precursor cells was detected in *foo/foo* embryos indicating that not all pharyngeal endoderm expression of *pax8* is dependent on *foo* activity (data not shown).

DISCUSSION

Role of *foxi one* in otic placode induction and organization

We have demonstrated that embryos mutated in *foo* show a severe defect in the formation of the otic placode. *foo* gene expression begins early with mRNA detectable by the sphere stage in a restricted ventral region near the animal pole. By fate mapping, this region corresponds to presumptive placodal tissue (Kozlowski et al., 1997; Woo et al., 1995). By the tail bud stage, *foo* expression was localized in two distinct bilateral regions that mark the future otic placodes. Prior to this study, *pax8* was the earliest known marker of the otic placodes. Remarkably, not only does *foo* expression in presumptive placodal tissue precede *pax8* expression, but *foo/foo* embryos also show a complete loss of *pax8* expression in the otic placode as well as reduction and disorganization of later otic placode markers. This places *pax8* downstream of *foo*, which makes it the earliest known marker of otic placode development and gives *foo* a demonstrated role in the induction of a specific otic vesicle marker.

At tail bud stage, *dlx3b* is normally expressed in all placodal tissue forming a discrete lateral band of expression that encircles the anterior neural plate with higher expression over the future otic placode (Akimenko et al., 1994). By the 10-somite stage, *dlx3b* is normally strongly expressed in the otic placode, although its expression is no longer detected laterally between the otic placode and the anteriormost domain. Although 10 somites stage *foo/foo* embryos show the reduced otic placode expression of *dlx3b*, the mutant embryos apparently also retain from the tail bud stage some of the lateral band of *dlx3b* expression surrounding the anterior neural plate (see Fig. 3), suggesting that *foo* may function in restricting or maintaining the coherence of the expression domains of placodal markers. This failure to tightly restrict the expression domains of otic placode markers such as *dlx3b* and *pax2a* might explain why *foo/foo* embryos often display split and/or duplicated otic vesicles at pharyngula and later stages. Thus, this Foxi1-dependent pathway has an essential function for the developing otic placode but not a significant role in initial induction.

Three recent papers show that induction of the otic placode requires both *fgf3* and *fgf8* (Leger and Brand, 2002; Maroon et al., 2002; Phillips et al., 2001). The combined data from the three papers suggest that *pax8* expression is induced by *fgf3* signaling, but the amount of signal required to induce *pax8* is much lower than other otic placode markers.

Removing *fgf3/8* signals completely eliminates otic induction, but *foo/foo* embryos still show an induction of several markers. Although other models are possible, the simplest model places *foo* activity between *fgf3/8* and *pax8* in the induction. Because of the observed phenotype, we propose that *fgf3/8* signaling to the otic placode induces parallel pathways. The Foxi1-independent pathway begins very early and would be responsible for the initial induction and expansion of the otic placode. As *foo/foo* embryos completely lacked *pax8* expression in the otic placode, yet were still able to induce placodal structures that ultimately formed an ear, our data suggests that in zebrafish, *pax8* and *foo* function are not required for otic placode induction. There is early *pax8* expression in mouse otic placodes (Pfeffer et al., 1998), and a mouse line with a targeted deletion of *pax8* has been made, but there no data have yet been reported regarding ear defects in these mice (Mansouri et al., 1998).

The second, Foxi1-dependent pathway has at least the one downstream effect: that of inducing *pax8* expression. Based on data obtained by treating embryos with the Fgf receptor inhibitor SU5402 (Leger and Brand, 2002), initiation of this *pax8* induction would take place sometime after 70% epiboly, as SU5402 added at 70% epiboly can block *pax8* expression. The role of the earlier initiating Fgf signal would be to provide an activating signal for *foo*-expressing cells to induce *pax8* and perhaps other unidentified downstream genes. It is also important to note that *foo* expression is likely to be independent of *fgf3/8* signaling even though *pax8* expression is not.

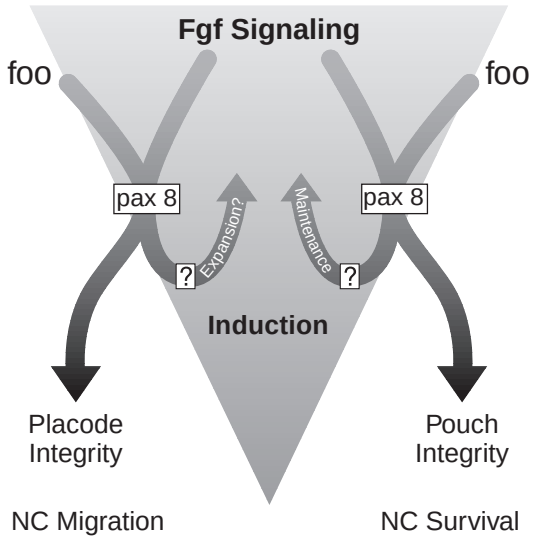

Fig. 10. A model that places *foo* in pathways for ear and jaw development. *foo* expression is independent of Fgf signaling, but it allows cells to respond to Fgf signaling with a specific genetic program, which includes the induction of *pax8*. Feedback mechanisms for the maintenance of Fgf expression are inferred from the data. Phenotypic effects observed in the embryos when *foo* function is eliminated are listed below.

We suggest that *foo/foo* mutant embryos demonstrate an uncoupling of otic placode induction from its subsequent morphogenesis (Fig. 10). This organizational or 'integrity-maintenance' activity would hold the placode together with the predicted effect of this model being similar to what we actually see in the *foo* mutants, that is, smaller dissociated placodal precursors. Because the regions of *pax2a* and *dlx3b* appear to be somewhat reduced, we also propose that *foo*-expressing cells generate positive feedback to the Fgf signals (Fig. 10). This is an idea we will return to more strongly in the discussion of the role of *foo* in the developing jaw.

Roles of *foo* in the developing jaw

We have demonstrated that *foo/foo* embryos display severe cartilage defects and shown how analysis of mutants provides mechanistic insight into how *foo* activity can differentially affect dorsal and ventral cartilage shapes through affecting the maintenance of *fgf3* expression. By the 10-somite stage, *foo/foo* embryos displayed a disorganized third stream of NC cells that invaded the otic placode region. As the otic placode is thought to serve as an inhibitory guidance cue (Sechrist et al., 1993; Smith et al., 1997), the observed third stream migration defect is perhaps secondary to the previously described otic placode defects. Without the maintained integrity of tight cell-cell interactions, the otic placode may no longer be capable of deflecting the ventral movement of third stream NC cells. The extent of the third stream migration defect appeared limited to invasion of otic placode territory because no *krox20*-expressing third stream cells were detected in post-migratory second stream territory (Fig. 4D, dorsal view, the area lateral to r2-r4). It is important to emphasize that a significant fraction of the third stream NC cells do not undergo apoptosis because, although reduced, posterior cartilages are readily detected in *foo/foo* embryos. Alternatively, these migration defects could be intrinsic to NC cells lacking Foo activity, a question that will require cell transplantations and cell autonomy studies for a clear answer.

Because first and second stream NC cell migration appeared normal in *foo/foo* embryos, the hyomandibular defects probably arose from defects at later stages of jaw development. By the 15-somite stage, *foo* expression was readily observed in the endoderm of the pharyngeal pouches. At around 20 somites stage, *foo/foo* embryos showed a loss of *pax8* expression from the pouches followed shortly at the 24 somites stage by a premature loss of *fgf3* expression. The combined action of strong Fgf signaling and *foo* activity would prefigure the pouch *pax8* expression domains, as *fgf3* is expressed in only the posterior half of pp2 as is *pax8*. Consistent with this observation, *pax8* expression in the otic placode is strongly dependent on both Fgf signaling and *foo* activity. Thus, in both the ear and the jaw, we propose that *foo* expression is responsible for the modification of downstream cellular responses to Fgf signaling leading to the induction of *pax8* expression.

Interestingly, loss of *pax8* expression in *foo/foo* embryos precedes the loss of *fgf3* maintenance in pp2. It is possible that *foo* and *pax8* function to maintain pouch endoderm integrity of markers such as *nkx2.3* in a manner analogous to otic placode integrity (Fig. 10). A future direction will be to determine whether feedback maintenance of Fgf signaling depends on *pax8* function.

fgf3 is expressed in the pharyngeal pouches in a roughly AP progressive wave. From 15 somites until around 34 hpf, *fgf3* expression is maintained in two pouches at a time with attenuation of the anterior-most pouch coinciding with the up regulation of the next posterior-most pouch. In *foo/foo* embryos, initial induction of *fgf3* expression in any particular pharyngeal pouch appeared to be only modestly affected. However, the onset of signal attenuation appeared prematurely, which is consistent with a role for *foo* in the maintenance of *fgf3* pouch expression. Thus, *foo* expression is not required for initial induction of *fgf3* in pouches but instead is part of a transient positive feedback mechanism that maintains *fgf3* signaling. It is possible that this maintenance is either at the transcriptional level causing cells to continue to express fgf3, or at the survival level, providing positive feedback signals that prevent fgf3 cells from apoptosis. Further experiments will be required to determine which of these is true.

At 26 hpf, a 20-fold increase in NC cell apoptosis was observed in the arches. This transient wave of cell death is probably a direct result of the lost *fgf3* maintenance because both *cas* mutants, which lack all endoderm (including *fgf3* pouch expression), and SU5402-treated embryos, in which Fgf receptor signaling is blocked, display extensive NC cell apoptosis. The apoptosis in *foo* mutant embryos is not as severe as these other cases because some residual *fgf3* signaling is still present. Consistently, *fgf3*-MO animals appear to display jaw defects that are very similar to and slightly more severe than those observed in *foo/foo* embryos (Figs 5, 8). Therefore, the failure to maintain *fgf3* expression in *foo/foo* embryos is what causes the widespread but transient NC cell apoptosis, causing reductions in the dorsal structures of both the mandibular and hyoid arches, and variable reductions in the more posterior branchial arches.

The apoptotic death of NC cells probably explains the later absence of the dorsal first and second arch *gsc* expression

domains as well as the loss of posterior arch defects in *dlx2*, *dlx3b* and *hand2* expression. Notably, *dlx2* expression is likewise lost in posterior arches of *cas/cas* and *fgf3*-MO animals (David et al., 2002). The unperturbed patterning of the ventral NC cells is indicated by the normal expression of *dlx2*, *dlx3b*, *hand2*, *gsc* and *hoxa2* gene expression in ventral NC cells as well as the equivalence in size of Meckel's cartilage between *foo/foo* and wild-type embryos. Interestingly, ventral NC cells of both the mandibular and hyoid arches do not require an *fgf3*-mediated signal for survival and/or proliferation, yet are absent in SU5402-treated embryos, implicating an essential role for a different as yet unidentified Fgf ligand. Similarly, it is worth noting that in spite of the *fgf3* maintenance defects, which extend into the more posterior pouches such as pp3 to pp5, that the most posterior fifth to seventh arches appear unaffected in *foo/foo* embryos. A possible explanation for the normal patterning of these posterior arches is an undetermined Fgf signal that can compensate for the loss of *fgf3*. Consistent with this explanation, *fgf3*-MO animals often show normal cartilages from the fifth to seventh arches that are missing in SU5402-treated embryos (David et al., 2002).

The complexity of the pharyngeal endoderm patterning pathways is further highlighted by the dual observations of lost pp2 *pax8* expression around the 20 somites stage (Fig. 9E,F) and retained thyroid follicular precursor cell *pax8* expression in 34 hpf *foo/foo* embryos (data not shown). As both tissues are pharyngeal endoderm derived, alternate pathways must exist for inducing *pax8* expression not only in tissues such as the eyes, MHB and pronephric ducts but also in more medial regions of the pharyngeal endoderm. It is possible or likely that *foo* expression in the pharyngeal pouches has other important functions that will require further experimentation to establish.

There are several noteworthy implications for the observed failure to maintain *fgf3* expression on possible mechanisms of establishing DV or AP polarity within an arch. First, it suggests that the relative size of a particular cartilage element can be directly influenced by the duration of a particular Fgf signal; the shorter the Fgf pulse, the fewer cells survive/proliferate and the smaller the structure. It is therefore possible that either a different Fgf signal might mediate survival of a different population of cartilage precursors or that a short but intense pulse of an Fgf signal could facilitate survival near the point source but with little effect at a distance. Second, it suggests that regional functionality of Fgf signaling could direct cartilage shape. The patterned induction of a variety of Fgf antagonist molecules, such as *sef* or *sprouty* family members, could direct cartilage shape by eliminating specific Fgf signals from specific NC cells. In support of this, *sprouty4* has been shown to be expressed in the pouches (Furthauer et al., 2001). The combined action of multiple patterned Fgf agonists and multiple antagonists could therefore generate fairly complex DV, AP and ML matrixes of survival, proliferation and death cues. Furthermore, we suggest small changes in this complex interplay of signals could be one of the mechanisms for the evolutionary adaptation of jaw structures.

Evolutionary implications

Our results show that in zebrafish, *foo* is a very early regulator of both ear and jaw development and is upstream of *pax8* induction in both structures. *pax2*, *pax5* and *pax8* are believed to have arisen from a single ancestral *pax2/5/8* gene (Pfeffer et al., 1998). Two recent publications have identified a single *pax2/5/8* gene in ascidians and amphioxus that is expressed in the region of the primordial pharynx, a region analogous to the pharyngeal arches of vertebrates (Kozmik et al., 1999; Wada et al., 1998). Given the observed commonality of gene expression between the otic vesicle and the arches, we argue for a synthesis between two interpretations of the *pax2/5/8* expression data in these primitive organisms (Kozmik et al., 1999; Wada et al., 1998). The ascidian cupulae could be considered gill slits that developed a placode-like function that differentiates into the ciliated primary sensory cells involved in feeding. The functional and spatial separation of these sensory regions away from the underlying arches as chordates evolved might explain why certain molecular markers that characterized the original gill slit ectoderm are maintained in vertebrate placode-derived structures. Because at least one vertebrate, the zebrafish, co-expresses *foo* and *pax8* in the otic placode ectoderm and also in the pouch endoderm, one might imagine that the primordial gill slit would express *foo* and *pax8* in both ectoderm and endoderm layers. The ability to perform gene knockdown studies in ascidians will allow for direct testing of conservation of gene regulatory networks (Heasman, 2002; Satou et al., 2001).

Even if the jaw and ear do not have a common origin, sharing gene regulatory networks helps explain how, across the water-to-land transition, the hyomandibular might transform into the stapes (Webster et al., 1992). If the hyoid NC cells lost purpose in the jaw but were still responsive to many of the same signaling molecules, such as Fgfs, then it is possible that the presumptive hyoid NC cells began responding to signals relating to the otic placode instead of the forming jaw. Without the similarities in gene expression, the mechanism for this jaw to middle ear NC cell shift would have to have happened in a more random and uncontrolled way. To address this issue directly is challenging; however, a simple, testable prediction of this jaw-ear crossover theory is that *Foxi1*$^{-/-}$ mice should display middle ear bone defects, perhaps specific to the stapes.

We thank Kirsten Sadler for critical reading of the manuscript; J. G. Crump, L. Maves and C. B. Kimmel for helpful discussions; B. Riley for fgf3-MO; and S. Farrington and the technical staff of the Hopkins laboratory for support. We also thank the Developmental Studies Hybridoma Bank (maintained by the Department of Biological Sciences, The University of Iowa) for the zn-8 antibody, and A. M. Caron of the MIT CCR Core Histology Facility for technical assistance on sections. R.M.N. was supported by a post-doctoral fellowship from the NIH. This work was also supported by grants from Amgen and NIH, and the intramural program of the NHGRI.

REFERENCES

Akimenko, M. A., Ekker, M., Wegner, J., Lin, W. and Westerfield, M. (1994). Combinatorial expression of three zebrafish genes related to distal-less: part of a homeobox gene code for the head. *J. Neurosci.* **14**, 3475-3486.

Alexander, J., Rothenberg, M., Henry, G. L. and Stainier, D. Y. (1999). casanova plays an early and essential role in endoderm formation in zebrafish. *Dev. Biol.* **215**, 343-357.

Amsterdam, A., Burgess, S., Golling, G., Chen, W., Sun, Z., Townsend, K., Farrington, S., Haldi, M. and Hopkins, N. (1999). A large-scale insertional mutagenesis screen in zebrafish. *Genes Dev.* **13**, 2713-2724.

Angelo, S., Lohr, J., Lee, K. H., Ticho, B. S., Breitbart, R. E., Hill, S., Yost, H. J. and Srivastava, D. (2000). Conservation of sequence and expression of Xenopus and zebrafish dHAND during cardiac, branchial arch and lateral mesoderm development. *Mech. Dev.* **95**, 231-237.

Avraham, K. B., Fletcher, C., Overdier, D. G., Clevidence, D. E., Lai, E., Costa, R. H., Jenkins, N. A. and Copeland, N. G. (1995). Murine chromosomal location of eight members of the hepatocyte nuclear factor 3/fork head winged helix family of transcription factors. *Genomics* **25**, 388-393.

Bever, M. M. and Fekete, D. M. (2002). Atlas of the developing inner ear in zebrafish. *Dev. Dyn.* **223**, 536-543.

Chen, W., Burgess, S., Golling, G., Amsterdam, A. and Hopkins, N. (2002). High-throughput selection of retrovirus producer cell lines leads to markedly improved efficiency of germ line-transmissible insertions in zebra fish. *J. Virol.* **76**, 2192-2198.

Clevidence, D. E., Overdier, D. G., Tao, W., Qian, X., Pani, L., Lai, E. and Costa, R. H. (1993). Identification of nine tissue-specific transcription factors of the hepatocyte nuclear factor 3/forkhead DNA-binding-domain family. *Proc. Natl. Acad. Sci. USA* **90**, 3948-3952.

Clouthier, D. E., Hosoda, K., Richardson, J. A., Williams, S. C., Yanagisawa, H., Kuwaki, T., Kumada, M., Hammer, R. E. and Yanagisawa, M. (1998). Cranial and cardiac neural crest defects in endothelin-A receptor-deficient mice. *Development* **125**, 813-824.

David, N. B., Saint-Etienne, L., Tsang, M., Schilling, T. F. and Rosa, F. M. (2002). Requirement for endoderm and FGF3 in ventral head skeleton formation. *Development* **129**, 4457-4468.

Ekker, S. C. (2000). Morphants: a new systematic vertebrate functional genomics approach. *Yeast* **17**, 302-306.

Furthauer, M., Reifers, F., Brand, M., Thisse, B. and Thisse, C. (2001). sprouty4 acts in vivo as a feedback-induced antagonist of FGF signaling in zebrafish. *Development* **128**, 2175-2186.

Golling, G., Amsterdam, A., Sun, Z., Antonelli, M., Maldonado, E., Chen, W., Burgess, S., Haldi, M., Artzt, K., Farrington, S. et al. (2002). Insertional mutagenesis in zebrafish rapidly identifies genes essential for early vertebrate development. *Nat. Genet.* **31**, 135-140.

Haddon, C. and Lewis, J. (1996). Early ear development in the embryo of the zebrafish, Danio rerio. *J. Comp. Neurol.* **365**, 113-128.

Hanneman, E., Trevarrow, B., Metcalfe, W. K., Kimmel, C. B. and Westerfield, M. (1988). Segmental pattern of development of the hindbrain and spinal cord of the zebrafish embryo. *Development* **103**, 49-58.

Hauptmann, G. and Gerster, T. (1995). Pou-2 – a zebrafish gene active during cleavage stages and in the early hindbrain. *Mech. Dev.* **51**, 127-138.

Heasman, J. (2002). Morpholino oligos: making sense of antisense? *Dev. Biol.* **243**, 209-214.

Hulander, M., Wurst, W., Carlsson, P. and Enerback, S. (1998). The winged helix transcription factor Fkh10 is required for normal development of the inner ear. *Nat. Genet.* **20**, 374-376.

Kimmel, C. B., Ballard, W. W., Kimmel, S. R., Ullmann, B. and Schilling, T. F. (1995). Stages of embryonic development of the zebrafish. *Dev. Dyn.* **203**, 253-310.

Kimmel, C. B., Miller, C. T. and Moens, C. B. (2001). Specification and morphogenesis of the zebrafish larval head skeleton. *Dev. Biol.* **233**, 239-257.

Kozlowski, D. J., Murakami, T., Ho, R. K. and Weinberg, E. S. (1997). Regional cell movement and tissue patterning in the zebrafish embryo revealed by fate mapping with caged fluorescein. *Biochem. Cell Biol.* **75**, 551-562.

Kozmik, Z., Holland, N. D., Kalousova, A., Paces, J., Schubert, M. and Holland, L. Z. (1999). Characterization of an amphioxus paired box gene, AmphiPax2/5/8: developmental expression patterns in optic support cells, nephridium, thyroid-like structures and pharyngeal gill slits, but not in the midbrain-hindbrain boundary region. *Development* **126**, 1295-1304.

Krauss, S., Johansen, T., Korzh, V. and Fjose, A. (1991). Expression of the zebrafish paired box gene pax[zf-b] during early neurogenesis. *Development* **113**, 1193-1206.

Kurihara, Y., Kurihara, H., Suzuki, H., Kodama, T., Maemura, K., Nagai, R., Oda, H., Kuwaki, T., Cao, W. H., Kamada, N. et al. (1994). Elevated blood pressure and craniofacial abnormalities in mice deficient in endothelin-1. *Nature* **368**, 703-710.

Larsson, C., Hellqvist, M., Pierrou, S., White, I., Enerback, S. and Carlsson, P. (1995). Chromosomal localization of six human forkhead genes, freac-1 (FKHL5), -3 (FKHL7), -4 (FKHL8), -5 (FKHL9), -6 (FKHL10), and -8 (FKHL12). *Genomics* **30**, 464-469.

Le Douarin, N. M. and Ziller, C. (1993). Plasticity in neural crest cell differentiation. *Curr. Opin. Cell Biol.* **5**, 1036-1043.

Lee, K. H., Xu, Q. and Breitbart, R. E. (1996). A new tinman-related gene, nkx2.7, anticipates the expression of nkx2.5 and nkx2.3 in zebrafish heart and pharyngeal endoderm. *Dev. Biol.* **180**, 722-731.

Leger, S. and Brand, M. (2002). Fgf8 and Fgf3 are required for zebrafish ear placode induction, maintenance and inner ear patterning. *Mech. Dev.* **119**, 91.

Lun, K. and Brand, M. (1998). A series of no isthmus (noi) alleles of the zebrafish pax2.1 gene reveals multiple signaling events in development of the midbrain-hindbrain boundary. *Development* **125**, 3049-3062.

Mansouri, A., Chowdhury, K. and Gruss, P. (1998). Follicular cells of the thyroid gland require Pax8 gene function. *Nat. Genet.* **19**, 87-90.

Maroon, H., Walshe, J., Mahmood, R., Kiefer, P., Dickson, C. and Mason, I. (2002). Fgf3 and Fgf8 are required together for formation of the otic placode and vesicle. *Development* **129**, 2099-2108.

Miller, C. T., Schilling, T. F., Lee, K., Parker, J. and Kimmel, C. B. (2000). sucker encodes a zebrafish Endothelin-1 required for ventral pharyngeal arch development. *Development* **127**, 3815-3828.

Nasevicius, A. and Ekker, S. C. (2000). Effective targeted gene 'knockdown' in zebrafish. *Nat. Genet.* **26**, 216-220.

Oxtoby, E. and Jowett, T. (1993). Cloning of the zebrafish krox-20 gene (krx-20) and its expression during hindbrain development. *Nucleic Acids Res.* **21**, 1087-1095.

Pfeffer, P. L., Gerster, T., Lun, K., Brand, M. and Busslinger, M. (1998). Characterization of three novel members of the zebrafish Pax2/5/8 family: dependency of Pax5 and Pax8 expression on the Pax2.1 (noi) function. *Development* **125**, 3063-3074.

Phillips, B. T., Bolding, K. and Riley, B. B. (2001). Zebrafish fgf3 and fgf8 encode redundant functions required for otic placode induction. *Dev. Biol.* **235**, 351-365.

Roehl, H. and Nusslein-Volhard, C. (2001). Zebrafish pea3 and erm are general targets of FGF8 signaling. *Curr. Biol.* **11**, 503-507.

Satou, Y., Imai, K. S. and Satoh, N. (2001). Action of morpholinos in Ciona embryos. *Genesis* **30**, 103-106.

Schulte-Merker, S., Hammerschmidt, M., Beuchle, D., Cho, K. W., de Robertis, E. M. and Nusslein-Volhard, C. (1994). Expression of zebrafish goosecoid and no tail gene products in wild-type and mutant no tail embryos. *Development* **120**, 843-852.

Sechrist, J., Serbedzija, G. N., Scherson, T., Fraser, S. E. and Bronner-Fraser, M. (1993). Segmental migration of the hindbrain neural crest does not arise from its segmental generation. *Development* **118**, 691-703.

Smith, A., Robinson, V., Patel, K. and Wilkinson, D. G. (1997). The EphA4 and EphB1 receptor tyrosine kinases and ephrin-B2 ligand regulate targeted migration of branchial neural crest cells. *Curr. Biol.* **7**, 561-570.

Solomon, K. S. and Fritz, A. (2002). Concerted action of two dlx paralogs in sensory placode formation. *Development* **129**, 3127-3136.

Sun, Z. and Hopkins, N. (2001). vhnf1, the MODY5 and familial GCKD-associated gene, regulates regional specification of the zebrafish gut, pronephros, and hindbrain. *Genes Dev.* **15**, 3217-3229.

Thisse, C., Thisse, B., Halpern, M. E. and Postlethwait, J. H. (1994). Goosecoid expression in neurectoderm and mesendoderm is disrupted in zebrafish cyclops gastrulas. *Dev. Biol.* **164**, 420-429.

Trainor, P. A. and Krumlauf, R. (2001). Hox genes, neural crest cells and branchial arch patterning. *Curr. Opin. Cell Biol.* **13**, 698-705.

Veitch, E., Begbie, J., Schilling, T. F., Smith, M. M. and Graham, A. (1999). Pharyngeal arch patterning in the absence of neural crest. *Curr. Biol.* **9**, 1481-1484.

Wada, H., Saiga, H., Satoh, N. and Holland, P. W. (1998). Tripartite organization of the ancestral chordate brain and the antiquity of placodes: insights from ascidian Pax-2/5/8, Hox and Otx genes. *Development* **125**, 1113-1122.

Webster, D., Popper, A. N. and Fay, R. R. (1992). *The Evolutionary Biology of Hearing*. New York: Springer.

Whitfield, T. T., Riley, B. B., Chiang, M. Y. and Phillips, B. (2002). Development of the zebrafish inner ear. *Dev. Dyn.* **223**, 427-458.

Woo, K., Shih, J. and Fraser, S. E. (1995). Fate maps of the zebrafish embryo. *Curr. Opin. Genet. Dev.* **5**, 439-443.